

# Stimuli-responsive luminescent solar concentrators based on photo-reversible polymeric systems

*Giovanni Fortunato, Elisavet Tatsi, Francesca Corsini, Stefano Turri, and Gianmarco Griffini\**

Department of Chemistry, Materials and Chemical Engineering “Giulio Natta”, Politecnico di Milano, Piazza Leonardo da Vinci 32, 20133 Milano, Italy.

**KEYWORDS:** stimuli-responsive polymers, photo-healable polymers, [2+2] cycloaddition, fluorescent coatings, luminescent solar concentrators

## ABSTRACT

Luminescent solar concentrators (LSCs) consist of dye-doped, highly transparent, plastic plates aimed at improving the building integration and reducing the cost of photovoltaic (PV) technology. In the thin-film configuration, the surface of these devices is particularly exposed to mechanical damage and to a consequent loss of performance in terms of power conversion. To address this issue, the first demonstration of a healable thin-film LSC based on a photo-reversible polymer network as the host matrix is presented in this work. The photo-responsive matrix is obtained by simple UV curing of a coumarin functional polyurethane through reversible [2+2] cycloaddition. The final crosslinked coating is optically clear and exhibits excellent scratch remendability after suitable UVC/UVA exposure. The LSC devices obtained by doping the responsive matrix with perylene- or

coumarin-based organic dyes possess a remarkable PV performance, comparable with control devices based on poly(methyl methacrylate). The loss of performance induced by surface mechanical scratches can be fully recovered by UV irradiation, as a result of the photo-reversibility of the coumarin functional polymer network. The healing strategy presented here, purely light triggered, expands the tools for the design of durable and responsive thin-film LSCs.

## 1. Introduction

The growing shift towards renewable resources for energy production has recently raised again the interest in photovoltaic (PV) technologies. Their efficient integration into existing buildings is one of the key challenges to be faced in order to meet the growing global demand of electricity.<sup>1</sup> In this context, luminescent solar concentrators (LSCs) represent a practical solution to this issue, owing to their transparency, easy color and shape tuneability, and direct production from available structural materials (typically glass or commodity polymers).<sup>2-4</sup> An LSC device is essentially made of a transparent material (i.e., the host matrix) doped with a luminescent species, or luminophore, able to harvest incident solar light by absorption. A fraction of the photons emitted by the luminophore (usually by fluorescence) remains trapped within the matrix, as the latter has higher refractive index than the surrounding environment (air), and is conveyed towards the edges of the device and collected by small-area PV cells.<sup>5</sup> The whole photon collection process is not exempt of loss events, which strongly affect the performance of the device. In this context, an ideal luminophore should provide a broad light collection, possess a high luminescent quantum yield (LQY) and a large Stokes shift in order to minimize self-absorption.<sup>6</sup> To meet these demands, a wide variety of dopants, mainly organic dyes, inorganic quantum dots and transition-metal complexes, have been developed in the last decades.<sup>7-10</sup> The host matrix plays a crucial role as well, since it should be highly transparent in order to minimize parasitic absorption, have a high refractive index ( $> 1.5$ ) and a homogeneous surface in order to avoid reflection and scattering phenomena, and should efficiently disperse the luminophore.<sup>5</sup> Conventional thermoplastics such as polyacrylates (in particular poly(methyl methacrylate) - PMMA) and polycarbonates usually meet those requirements and thus represent a common and cheap choice for the design of LSC devices.<sup>5,11</sup>

A real-life implementation of these matrices raises the issue of durability of such LSC devices in outdoor environment. In fact, weathering caused by environmental agents like radiation, oxygen, moisture, dust and mechanical damages can significantly degrade the polymer matrix, resulting in a reduction in the smoothness of device surface, a consequent loss of performance,<sup>12,13</sup> and, eventually,

the failure of the coating.<sup>14</sup> In light of this, some strategies to overcome mechanical damages of LSCs during outdoor service life have recently been proposed. Among these, laminated LSCs, in which a covering glass is applied onto the LSC top surface, appear to be an interesting practical solution. Indeed, glass lamination not only avoids the mechanical scratching of the active layer, but also protects it from direct exposure to the surrounding environment.<sup>15–19</sup> However, due to the decrease of the concentration factor, larger PV cells are typically required on the edges of the laminated LSCs, which might have an effect on the cost of generated electricity (€/kWh)<sup>17</sup>. Also, part of the incident light (mostly in the UV region) could be cut off from the covering glass, thus partly reducing the number of photons potentially harvested by the luminophore in that wavelength range. Alternatively, functional host matrices are clearly advantageous over commodity plastics. For example, extended photochemical stability and self-cleaning ability were imparted to a LSC device by designing a functional host matrix based on crosslinked fluoropolymers doped with a perylene dye.<sup>20,21</sup> Within this context, the self-healing function could extend the lifetime of LSC devices, particularly those in thin-film configuration, which are more prone to mechanical damage with respect to bulk configuration devices owing to their high surface/thickness ratio.<sup>22</sup>

Self-healing coatings are a class of smart coatings able to repair small mechanical damages autonomously (typically by the rupture of microcapsules containing the healing agent) or in response to a suitable stimulus in the form of heat or radiation (non-autonomous mechanism).<sup>23–27</sup> Within this context, the radiation stimulus (visible or UV light) offers the possibility of a temporal and spatial control of the healing process typically not easy with thermally induced healing.<sup>28,29</sup> UV-induced self-healing is based on the reversible dimerization *via* [2+2] cycloaddition of specific photo-responsive groups such as coumarin, cinnamoyl, anthracene or thymine derivatives. Dimerization is achieved by irradiating the species in solution or in the solid state at  $\lambda > 350$  nm, while upon irradiating the dimers at lower wavelength (typically 254 nm) bond cleavage is favored.<sup>30</sup> Thus, a photo-reversible polymer network can be obtained by incorporating in a linear chain photo-responsive groups acting as crosslinkers. Since the network has reversible nature, the material increases its mobility during UVC

irradiation and toughens again under UVA/visible light, allowing repair of damaged surfaces. In particular, coumarin derivatives, owing to the wide availability of their precursors and their easy functionalization, represent a convenient platform for the design of photo-responsive polymers<sup>31</sup> for applications in various fields, including resists in nanoimprint lithography,<sup>32</sup> controlled drug release,<sup>33–35</sup> and self-healing films or coatings.<sup>36–47</sup>

Based on these considerations, in this work, the first demonstration of UV-triggered self-healing polymer for thin-film LSC applications is reported. A coumarin-functionalized macromer, obtained from a one-step modification of a polyisocyanate prepolymer, was crosslinked under UVA light to yield a highly transparent and colorless coating. Owing to its excellent photo-reversibility, evaluated from absorption and fluorescence spectroscopy, the system was able to successfully heal upon mechanical damage, under a suitable UVC/UVA light irradiation cycle. Embedding the dimer-based matrix with a perylene or a coumarin derivative allowed to obtain LSC devices with efficiency comparable with reference state of the art systems. Moreover, a purely photo-induced healing of the damaged surface of the device resulted in a complete recovery of the original performance.

## 2. Experimental Section

*Materials:* 7-Hydroxy-4-methylcoumarin (HMC), 2-bromoethanol, dibutyltin dilaurate (DBTDL), N,N-dimethylformamide (DMF), ethyl acetate and chloroform were obtained from Sigma-Aldrich and used as received. Potassium carbonate was obtained from CARLO ERBA Reagents. Desmodur® XP 2599 (DX2599, aliphatic isocyanate prepolymer with 6.0 wt.% NCO, average functionality of 4.2) was kindly provided by Covestro. Lumogen® F Red 305 (LR305) was supplied by BASF and Coumarin 6 (C6), more specifically 3-(2-Benzothiazolyl)-7-(diethylamino) coumarin, by TCI chemicals. PMMA (ALTUGLAS® BS 550) and index matching liquid 150 (IML150) were purchased from Arkema and Norland, respectively. Monocrystalline high efficiency silicon solar cells were provided by IXYS (IXOLAR SolarBIT KXOB22-12X1F, active area  $2.2 \times 0.6 \text{ cm}^2$ ,  $V_{OC} = 0.64$

$\pm 0.01$  V,  $J_{SC} = 42.60 \pm 0.42$  mA cm<sup>-2</sup>, FF =  $69.4 \pm 0.3\%$ , power conversion efficiency (PCE) =  $18.69 \pm 0.23\%$ ).

*Synthesis of 7-(hydroxy ethoxy)-4-methylcoumarin (HEOMC):* HEOMC was synthesized according to a reported procedure with some modifications.<sup>17a</sup> Typically, HMC (8 g, 45.4 mmol) was dissolved in 50 ml DMF in a round bottom flask equipped with a magnetic stirrer. Upon addition of 2-bromoethanol (8.6 g, 68.8 mmol) and potassium carbonate (12.6 g, 91.2 mmol), the flask was sealed and put under inert atmosphere through evacuation-backfilling with nitrogen. The mixture was stirred for 18 h at 90 °C, cooled down to room temperature and poured into 150 ml ice water. The solid was collected through filtration and recrystallized twice from ethyl acetate, to give a yellow powder. Yield = 78%; mp 149 °C; IR (KBr):  $\nu$  = 3439 (s;  $\nu_s$ (O–H)), 3069 (w,  $\nu_s$ (aromatic C–H)), 2955, 2931 (w,  $\nu_s$ (aliphatic C–H)), 1701 (s,  $\nu_s$ (C=O)), 1621 (s,  $\nu_s$ (C=C pyrone ring)), 1555, 1388 (m, aromatic  $\nu_s$ (C=C)) 1153, 1076 cm<sup>-1</sup> (m,  $\nu_s$ (C–O)). <sup>1</sup>H NMR (400 MHz, DMSO- *d*<sub>6</sub>,  $\delta$ ): 7.65 (m, 1H, Ar–H), 6.95 (m, 2H, Ar–H), 6.18 (d, *J* = 1.2 Hz, 1H, C=C–H), 4.92 (br, 1H, –OH), 4.09 (t, *J* = 4.9 Hz, 2H, –CH<sub>2</sub>–), 3.73 (t, *J* = 4.9 Hz, 2H, –CH<sub>2</sub>–), 2.38 (d, *J* = 1.1 Hz, 3H, –CH<sub>3</sub>)

*Synthesis of coumarin urethane prepolymer (PU-Cou):* Desmodur® XP 2599 (7.3 g, 10.4 mmol of NCO) was weighed into a two-necked round bottom flask equipped with a magnetic stirrer. The flask was sealed with a rubber septum and heated for 1 h at 70 °C, under dynamic vacuum, in order to dry the prepolymer. Upon cooling down to rt, the flask was filled with nitrogen and a solution of HEOMC (2.30 g, 10.4 mmol) in 80 mL chloroform was added. DBDTL (1 wt. % with respect to dry reagents) was injected and stirring was continued for 2 h at room temperature (rt), under inert atmosphere. The reaction was monitored by following the disappearance of 2270 cm<sup>-1</sup> band (NCO stretching in isocyanates) in FTIR spectra. Solvent was removed under vacuum and the residual solids were re-dissolved in THF (10 wt. %). Insoluble particles (unreacted HEOMC) were separated by centrifugation, while the supernatant was dried in a vacuum oven (50 °C, 24 h) to give a waxy, white solid. Yield = 92%.

*Coating preparation and UV irradiation:* PU-Cou was spin coated (600 rpm, 60 s) from chloroform solutions (120 mg/ml) on glass or quartz slides using a Laurell WS-400BZ-6NPP/LITE instrument. The obtained samples were irradiated under a UV polymerization apparatus (Helios Quartz, POLIMER 400W) equipped with high-pressure mercury lamps. Specifically, crosslinking was performed using a UVA lamp (Zs type, Helios Quartz) with emission window between 315 and 400 nm and with radiative power density equal to 54.6 mW/cm<sup>2</sup>. Decrosslinking was performed under a UVC lamp (Zp type, Helios Quartz), with emission window between 100 and 400 nm equipped with a 254 nm bandpass filter (Omega Optical - 254nm CWL, Hard Coated OD Bandpass Filter), and a power density of 2.4 mW/cm<sup>2</sup>. Irradiations were performed both in air and inert atmosphere (flux of nitrogen).

*LSC device fabrication:* LSCs were fabricated in thin-film configuration starting from chloroform solutions of PU-Cou macromer (120 mg/mL) with different concentrations of LR305 or C6 dyes (1-9 wt.% with respect to dry polymer). Films with average thickness  $\sim 1.5 \mu\text{m}$  were obtained by spin coating (600 rpm for 60 s) onto  $4.4 \times 4.4 \times 0.6 \text{ cm}^3$  glass slabs and UVA irradiation (120 min). LSCs were attached to two modules, each incorporating two monocrystalline silicon solar cells connected in series, by means of a low viscosity IML150 index matching liquid (viscosity 100 cP, refractive index  $\sim 1.52$ ), so that two opposite edges of the glass substrate faced the photoactive area of one PV module each.

*Structural and thermal characterization:* <sup>1</sup>H-NMR (400 MHz) spectra were recorded on a Bruker Avance 400 using deuterated DMSO as solvent. FTIR spectra were recorded using a Thermo Nicolet Nexus 670 instrument. Measurements were performed on solids coated on KBr discs, recording 64 accumulated scans at a resolution of 2 cm<sup>-1</sup>. GPC analyses were performed on an apparatus consisting in a Waters 515 HPLC pump (mobile phase, THF; flow rate, 1 mL/min, at 35 °C), three Styragel columns (models HR 4, HR 3, and HR 2) from Waters, and a refractive index detector Waters 2410. Samples were dissolved in THF at concentrations of 0.2 wt. %. A calibration curve was prepared by using monodispersed fractions of polystyrene. Differential scanning calorimetry (DSC) analyses were

performed with a DSC 823e Mettler-Toledo instrument, by applying the following thermal cycle: from 25 °C to 180 °C, from 180 °C to -50 °C, and from -50 °C to 180 °C. Heating/cooling rate was 20 °C/min. Thermogravimetric analyses (TGA) were performed with a Q500 TGA system (TA Instruments) from rt to 800 °C at a scan rate of 10 °C/min in air atmosphere.

*Optical characterization:* UV–visible spectroscopy analyses were performed at rt on a Thermo Scientific Evolution 600 UV–vis spectrophotometer. Relative reflectance was measured on a Jasco V-570 UV-Vis-NIR spectrophotometer equipped with an integrating sphere and a PTFE foil as reference. Refractive index was measured using a Filmetrics F20 thin film analyzer in the wavelength range 400–800 nm and the BK7 reflection standard was used to calibrate the instrument in the contact stage mode. The samples for refractive index analysis were prepared by spin coating (600 rpm, 60 s) a chloroform solution of PU-Cou (80 mg/mL) on a silicon wafer substrate followed by UVA irradiation for crosslinking. Fluorescence spectra were recorded on a Jasco FP-6600 spectrofluorometer. Photoluminescence quantum yield of crosslinked PU-Cou was measured on a FluoroMax-2 spectrofluorometer equipped with an R928 photomultiplier tube. Optical and fluorescence micrographs were recorded through a Leica DMI3000B fluorescence microscope equipped with a digital camera, by using specific filters depending on the excitation and emission wavelengths of the investigated samples. Device efficiency measurements were performed using an Abet Technologies Sun 2000 solar simulator with AM1.5G filter and a spectroradiometer (International Light Technologies ILT950) to collect the edge emission of the LSC. The power emission spectra of the LSCs were recorded using Spectralight software, calibrated by the manufacturer to give the spectral distribution in units of power ( $\mu\text{W}$ ). A Keithley 2612B source-measuring unit was used to perform the voltage scans and measure the current output. The data obtained were averaged out of at least three different devices.

*Photochemical stability and surface properties:* Weathering tests were performed in a Solarbox 3000e weather-o-meter chamber (Cofomegra srl), equipped with a Xenon lamp and an outdoor filter ( $\lambda > 280 \text{ nm}$ ). The total applied irradiance was equal to  $550 \text{ W/m}^2$  in the 300–800 nm range at a



temperature of 40 °C and an average relative humidity of 25%. Adhesion strength of the coatings on glass substrates was determined through a PosiTest AT-M Manual pull-off tester (DeFelsko) by measuring the pulling force needed to detach a 20 mm-diameter aluminum dolly glued to the crosslinked coatings by means of a two-component epoxy adhesive (Araldite 2011, curing cycle: 50 °C, 24 h). Wettability was studied in terms of static optical contact angle (OCA) measurements, which were performed with an OCA 20 (DataPhysics) equipped with a CCD photo-camera and with a 500  $\mu$ L Hamilton syringe to dispense liquid droplets. Water and diiodomethane ( $\text{CH}_2\text{I}_2$ ) were used as probe liquids. The surface energy of the coatings was calculated according the Owens-Wendt-Rabel-Kaelble (OWRK) method.<sup>48</sup>

### 3. Results and Discussion

#### 3.1. Synthesis and characterization of coumarin-functionalized polyurethane (PU-Cou)

The photo-responsive polyurethane was obtained by a one-step reaction between a commercial aliphatic isocyanate prepolymer (Desmodur® XP 2599, from here on referred to as DX2599) and a coumarin derivative (7-(hydroxy ethoxy)-4-methylcoumarin, HEOMC) (**Scheme 1A**). Since aliphatic alcohols exhibit higher reactivity towards isocyanate addition compared to aromatic ones,<sup>49</sup> 7-hydroxy-4-methylcoumarin (HMC) was reacted with 2-bromoethanol in order to obtain an aliphatic alcohol (HEOMC).<sup>36</sup> Indeed, the reaction was complete in 2 h at rt and the coumarin-modified prepolymer (PU-Cou) was obtained in excellent yield. The modification was studied by FTIR spectra (**Figure 1A** and Figure S1 in Supporting Information). Specifically, the signals at 3440  $\text{cm}^{-1}$  (O–H stretching) and 2270  $\text{cm}^{-1}$  (N=C=O stretching) associated to HEOMC and isocyanate precursor respectively are absent in the final product, confirming full conversion of isocyanate and alcohol groups. Moreover, the peaks appearing in the PU-Cou spectrum at 3075  $\text{cm}^{-1}$  (unsaturated C–H stretching), 1618  $\text{cm}^{-1}$  (C=C stretching in pyrone rings), 1152  $\text{cm}^{-1}$  (C–H bending in pyrone rings)<sup>50</sup> confirmed the incorporation of coumarin moieties in the prepolymer. GPC analyses evidenced a clear

increase in the number average molecular weight ( $M_n$ ) from 3210 g/mol for the isocyanate prepolymer to 4370 g/mol for PU-Cou, while polydispersity index ( $\mathcal{D}$ ) was around 1.1 for both the macromers, providing further confirmation of functionalization.

UV-Vis absorption spectrum (**Figure 1B**) of PU-Cou coated on quartz displayed a broad, intense signal around 320 nm, which is characteristic of substituted coumarins and related to overlapping  $\pi$ - $\pi^*$  electron transitions of conjugated benzene and pyrone chromophores.<sup>51</sup> Moreover, the fluorescence emission spectrum, with 320 nm as excitation wavelength, exhibited a broad band peaking at  $\lambda=394$  nm (blue region), which is typical of coumarin derivatives bearing electron donating groups in position 7, as the precursor HEOMC.<sup>52</sup>

### 3.2. Photo-induced crosslinking and characterization

The photo-reactivity of PU-Cou was studied by recording UV-Vis spectra of thin films spin coated on quartz slides after different time intervals of exposure under the UVA source ( $\lambda > 300$  nm). As evidenced in **Figure 2A**, the strong absorption signal around 320 nm gradually decreased with the irradiation time. As the double bonds of coumarin groups reacted to form the cyclobutane rings by [2+2] cycloaddition (Scheme 1B), the conjugation is progressively lost, leading to decrease in the absorbance.<sup>29,31</sup> The extent of the conversion of pendant coumarin groups into the photo-dimers (dimerization degree, DD%) was calculated according to the following equation:<sup>36</sup>

$$DD \% = \left(1 - \frac{A_t}{A_0}\right) \cdot 100 \quad (1)$$

where  $A_0$  and  $A_t$  are the absorption intensities at 320 nm before and after a time  $t$  of UV exposure, respectively. As shown in **Figure 2B**, the dimerization degree increases over time and reaches a plateau after 120 min of exposure, corresponding to conversion of 93.2%, in line with previously reported systems.<sup>37,53</sup> As reported in **Figure 2C**, the UVA treatment for 120 min (corresponding to maximum conversion of coumarin groups) strongly reduced the fluorescence intensity at 394 nm, owing to the decrease in concentration of luminophores in dimerized PU-Cou.<sup>54</sup> Nevertheless, the

decrease was only 68.8%, significantly lower than the one calculated from the absorbance spectra (93.2%). The difference can be explained by considering that a lower number of coumarin chromophores also results in a lower probability of re-absorption / re-emission events, as suggested by the slight blue shift in the fluorescence spectrum of dimerized PU-Cou with respect to as cast material.

Owing to the high functionality of PU-Cou (around 4.2 coumarin units per mole, based on the NCO/mole ratio of the parent polyisocyanate), the UVA photo-induced dimerization process of coumarin moieties is expected to yield photo-curing of the material. Indeed, upon UVA irradiation the soluble macromer turned into an insoluble, densely crosslinked network, as evidenced by gel content measurements. Specifically, PU-Cou was spin coated from chloroform solutions on glass slides and irradiated under UVA (120 min). The obtained samples, with an average thickness of 1.5  $\mu\text{m}$ , were immersed in chloroform for 24 h and the residual insoluble content was found to be > 95%, consistently with the dimerization degree calculated by UV-Vis spectroscopy.

An extensive characterization of crosslinked PU-Cou was performed in terms of thermal, optical and surface properties, in order to assess its relevance for optical coatings applications. As of thermal characterization, DSC traces evidenced a single glass transition ( $T_g$ ) at around 50 °C for the crosslinked polymer (see Figure S2 in Supporting Information), while pristine PU-Cou macromer displayed a broad melting transition around 70 °C, which was evidently suppressed after the UV-induced dimerization. The decomposition profile, measured by TGA in air, did not show any degradation event before 210 °C (Figure S3 in Supporting Information), thus demonstrating the excellent thermal stability of the crosslinked material.<sup>55</sup> As for the optical properties, coatings were visually clear and colorless after the UVA irradiation, with a transmittance greater than 90% in the 400-900 nm range (**Figure 2D**). Specifically, no discoloring was observed, owing to the inherent UV stability of aliphatic polyurethanes compared to aromatic ones.<sup>56</sup> Such high transparency was retained even during a long-term (> 500 h) accelerated weathering test under continuous white-light illumination (Figure S4 Supporting Information), clearly evidencing the excellent photostability of

the crosslinked PU-Cou system and confirming its potential suitability for outdoor use. Furthermore, the reflectance was as low as 8.0% over the 400-800 nm spectral range and the refractive index resulted to be 1.51 ( $\lambda = 589$  nm). Both values were close to those reported for commercial PMMA and, combined with its high transparency, demonstrated the suitability of crosslinked PU-Cou as a potential host matrix for LSCs.<sup>11</sup> The LQY of the crosslinked coatings resulted to be 26.7%. Regarding surface properties, static contact angle measurements evidenced a moderate hydrophobicity ( $\theta_{\text{H}_2\text{O}} = 93^\circ$ ) and a surface energy ( $\gamma = 46.12$  mN/m) predominantly determined by the dispersive component ( $\gamma_d = 46.01$  mN/m). Lastly, the adhesion strength on glass obtained from pull-off tests was found to be higher than 16 MPa, with cohesive failure in the glass substrate and no detachment of the coating. The value is particularly remarkable in view of the application of this material as functional coating for transparent substrates, e.g., on retrofitted windows.

### 3.3. Photo-induced network reversibility and self-healing

The crosslinked coatings were irradiated under monochromatic UVC light ( $\lambda = 254$  nm). As evidenced by the progressive increase of the absorption signal around 320 nm (**Figure 3A**) the photocleavage of cyclobutane adducts in the dimers restores the conjugation of the coumarin moieties (Scheme 1B). The DD% decreased over time reaching a plateau at 23% (**Figure 3B**), implying that the photo-cleavage was not complete. This feature is generally observed in coumarin-based photo-reversible polymer networks when irradiated in the solid state, and it is ascribed to a dynamic equilibrium between cycloaddition and its reverse.<sup>30,31,39</sup> Fluorescence emission spectra (**Figure 3C**) evidenced the high degree of recovery ( $\approx 85\%$ ) of the original emission intensity after UVC irradiation. FTIR analysis, performed on thin films coated on KBr crystal windows, allowed to monitor structural changes after the UVA/UVC irradiation cycles. In accordance with literature,<sup>36</sup> the spectrum of pristine, uncrosslinked PU-Cou presented two relevant signals in the 1800 – 1600  $\text{cm}^{-1}$  spectral range: the band centered at 1718  $\text{cm}^{-1}$  (C=O of pyrone ring overlapped with C=O in polyurethane) and the one at 1618  $\text{cm}^{-1}$  (C=C of pyrone ring overlapped with phenyl ring). Upon

UVA irradiation a shoulder peak appeared at  $1760\text{ cm}^{-1}$  while the band at  $1618\text{ cm}^{-1}$  decreased and shifted, indicating conversion of double bonds. The subsequent UVC irradiation allowed to restore the structural changes (**Figure 3D** and Figure S5 in Supporting Information).

Photo-induced dimerization and cleavage were performed cyclically, by alternating UVA and UVC irradiations (**Figure 4A**). The slight decrease in the efficiency of the dimerization/cleavage process upon repeated cycles is commonly observed in coumarin-based systems and attributed to side reactions during the 254 nm treatment, which cause the formation of non-reversible adducts and/or cleavage byproducts.<sup>30,39</sup> Nevertheless, the polymer network displayed high reversibility and recovery of fluorescence during multiple cycles (**Figure 4B**). Indeed, a full reversibility on a molecular scale is not a necessary condition for complete aesthetical and functional recovery of the coating surface, as confirmed by qualitative self-healing tests. The PU-Cou coating was crosslinked under UVA and its surface was damaged by means of a scalpel, producing scratches with average width of 30-40  $\mu\text{m}$  and depth lower than the coating thickness (**Figure 4C**). Upon exposure to UVC ( $\lambda = 254\text{ nm}$ , 160 min) followed by UVA ( $\lambda > 300\text{ nm}$ , 120 min), complete repair was observed (**Figure 4D**). Exposure times were established in order to maximize the number of free coumarin generated during the photocleavage and the number of dimer adducts during the photo-crosslinking stage, on the basis of the kinetics determined by UV-Vis spectroscopy. Two control experiments were performed in order to elucidate the specific role of [2+2] photocycloaddition in the repairability of the polymer matrix. First, when the damaged samples were directly irradiated for 5 h under UVA only, no healing was observed (Figure S6A in Supporting Information). This indicates that the sole mechanical damage, which is commonly considered to occur preferentially at the cyclobutane crosslinks, does not generate enough free coumarin moieties able to promote healing through UVA re-crosslinking. As a consequence, a preliminary UVC treatment for photocleavage is necessary in order to achieve the repair, in accordance with the majority of previously reported systems.<sup>29,36,38</sup> Secondly, when damaged samples were heated at  $60\text{ }^{\circ}\text{C}$  (*i.e.* above the  $T_g$ ) for 5 h in the dark, no healing was observed, pointing out that the sole thermal stimulus was not able to induce repair (Figure

S6B in Supporting Information). The photo-induced healing ability in the presence of multiple surface scratches was also investigated. As more extensively discussed in Section S.6 in the Supporting Information, optical microscopy and profilometric analyses proved the full repair of the PU-Cou coating after healing treatment (UVC+UVA). These results further demonstrate the excellent photo-induced healing ability of our system.

### 3.4. Dye incorporation and optical characterization

Given the excellent thermal, optical, and functional characteristics of this photo-responsive coumarin-based coating system, its suitability as host matrix material for LSC application was investigated by doping PU-Cou with two distinct fluorophores: Lumogen® F Red 305 (LR305) or Coumarin 6 (C6), selected because of their wide availability, high LQY (>95%) and broad Stokes shift.<sup>12</sup> In particular, LR305 represents the state-of-the-art in organic dopants for LSCs,<sup>2,57,58</sup> while C6, a widely used fluorescent dye,<sup>59</sup> only recently was proposed as luminescent dopant for this application.<sup>60</sup> Each dye was combined with PU-Cou in chloroform solution, spin coated on glass slabs and irradiated under UVA for 120 min, to ensure maximum crosslinking of the polymer matrix. The obtained coatings were visually clear and homogeneous. Upon immersing the coated slides in chloroform for 24 h under stirring, the dyes were completely extracted from the crosslinked PU-Cou coatings, as confirmed by UV-Vis spectroscopy (Figure S9 in Supporting Information). Thus, no chemical interaction between the embedded fluorescent dyes and the host matrix was found to occur during the UVA treatment to induce crosslinking.

To gain preliminary insights into the optical properties of the selected fluorophores, a first characterization by means of UV-Vis and fluorescence spectroscopy was performed on LR305 and C6 dispersed in a reference polymeric matrix (i.e., PMMA) subjected to the same UVA treatment used on PU-Cou coatings. The absorption spectrum of LR305/PMMA (**Figure 5A**) exhibited the two characteristic peaks of LR305 (445 nm and 575 nm), and a peak at 611 nm in the fluorescence emission spectrum, in accordance with literature.<sup>21,61</sup> As for C6/PMMA, the peak at 444-450 nm in

the absorption spectrum and the one at 539 nm in the emission profile (**Figure 5B**) are indicative of coumarin derivatives substituted with an amino group in the 7 position of the benzene ring, as in C6.<sup>52,62,63</sup> In addition, the spectral overlap of the absorption spectrum of the luminophore (acceptor species) with the emission spectrum of the undoped crosslinked PU-Cou coating (donor specie) suggested possible occurrence of energy transfer *via* fluorescence resonance mechanism (FRET) from the host matrix to the luminescent species.<sup>64–68</sup> Indeed, the values of spectral overlap integral (see Supporting Information for details on the calculation) resulted to be  $2.93 \cdot 10^{-14}$  and  $7.42 \cdot 10^{-15} \text{ cm}^3 \text{ M}^{-1}$  for LR305- and C6-doped PU-Cou, respectively, in line with those reported in the literature.<sup>69</sup> A deeper analysis of FRET mechanism is presented in the Supporting Information (Section S8).

UV-vis absorption spectra performed on LR305/PU-Cou highlighted the contribution of the absorption features of both the matrix and the dye (**Figure 6A**). Owing to the complete transparency of the crosslinked PU-Cou in the visible range, the characteristic peaks of the perylene-based dye could be clearly observed. Furthermore, by increasing the concentration of the dye from 1 wt% to 7 wt%, the absorbance ( $\lambda_{\text{max}} = 577 \text{ nm}$ ) linearly increased, while a progressively decreased solubility of LR305 in PU-Cou at higher concentrations caused deviation from linearity.

Fluorescence emission spectra ( $\lambda_{\text{exc}} = 327 \text{ nm}$ , recorded in front-face configuration) evidenced a strong emission signal peaking at 611 nm, contributed by both the matrix and the dye through energy transfer, as previously discussed. The intensity of the fluorescence peak was found to increase gradually with the absorbance up to  $A \approx 0.45$  (corresponding to 5 wt% LR305) while, above this threshold, a gradual decrease was observed (**Figure 6B**). Furthermore, a bathochromic shift of the emission peak was observed in normalized emission spectra (**Figure 6C**), typical of highly doped LSCs and ascribed to a higher probability of re-absorption processes and to aggregation of dye molecules<sup>39,70–72</sup>.

In contrast to what observed in LR305/PU-Cou systems, a markedly different optical behaviour was reported for C6/PU-Cou, resulting in maximum optical performance for 3 wt% C6 doping level (see Section S.12 in Supporting Information).

### 3.5. LSC device characterization and photo-induced healing

Considering the favorable optical characteristics of luminophore-doped PU-Cou self-healing coatings (5 wt.% LR305 or 3 wt.% C6), their performance as thin-film LSCs was evaluated in the presence of edge-coupled c-Si PV cells (see Experimental section for details) by calculating the so-called device efficiency ( $\eta_{LSC}$ ):<sup>60</sup>

$$\eta_{LSC} = \frac{FF \cdot I_{SC} \cdot V_{OC}}{P_{IN} \cdot A_{LSC}} \quad (2)$$

where  $A_{LSC}$  is the active (top) area of the LSC device,  $P_{IN}$  is the incident solar-simulated power density and  $FF$ ,  $I_{SC}$  and  $V_{OC}$  are the fill factor, the short-circuit current and the open-circuit voltage of the edge-coupled PV cells, respectively. In order to ensure reliability in the measurements, a dark absorbing background was used underneath the LSC slab and no reflective elements were placed at the free edges of the lightguide. In this way, reflections and back-scattered light from inside or outside the waveguide as well as multiple-pass of photons could be excluded, thus avoiding overestimation of the obtained results. In addition, direct illumination of the edge-mounted PVs was carefully prevented. In these experimental conditions, overall (four edges)  $\eta_{LSC}$  values as high as  $1.16 \pm 0.06$  % for LR305/PU-Cou and  $0.64 \pm 0.04$  % for C6/PU-Cou could be achieved, which are in line with recently reported results on other thin-film LSCs using similar fluorophores as luminescent species and tested in analogous conditions.<sup>73,74</sup> To assess the contribution of our UV-responsive self-healing matrix on the obtained PV performance, convenient benchmark LSC devices were obtained by coating glass slabs with doped PMMA, the latter being selected as reference host matrix given its wide use in the field. The concentration of LR305 and C6 in PMMA was adjusted in such a way to obtain LSCs with the same optical density (OD, evaluated at  $\lambda_{max}$ ) as those based on our PU-Cou matrix, namely  $OD \approx 0.61$  for LR305 and  $OD \approx 0.18$  for C6. In the same experimental conditions previously described, the  $\eta_{LSC}$  values of such PV-coupled LSCs were 1.20% for LR305/PMMA and 0.66% for C6/PMMA, thus comparable with the ones obtained with our photo-responsive systems.



This result further confirms the factual potential of PU-Cou as host matrix material for high efficiency LSCs.

Then, to evaluate the effect of surface damages on the performance of PV-coupled LSCs and to demonstrate the photo-induced healing ability of the new PU-Cou LSC system, tests were performed on scratched LSC coatings prior to and after UV healing treatment. As shown in **Figure 7**, by damaging the surface of the LSC with a scalpel to induce a single 20 - 30  $\mu\text{m}$  wide scratch, a non-negligible reduction of device performance could be observed compared with the pristine undamaged LSCs (namely a  $\sim 5\%$  and  $\sim 7\%$  loss in  $\eta_{LSC}$  for LR305-doped and C6-doped matrix, respectively). Indeed, an increase in surface roughness resulting from the mechanical damage determines a higher probability of light scattering events at defects generated on the coating surface, leading to a reduced ability to trap travelling photons within the host matrix. Upon UV-induced healing, namely by irradiating the damaged samples at 254 nm (160 min), followed by UVA ( $\lambda > 300$  nm) treatment for 120 min, complete disappearance of the surface scratches was reported from optical micrographs on both LR305- and C6-doped LSC systems, paired with a complete recovery ( $\sim 100\%$ ) of the original LSC performance (**Figure 7C** and **Figure 7E**). These results clearly demonstrate the excellent photo-induced healing capabilities of these systems also in the presence of a luminescent dopant, and provide evidence of their potential in restoring aesthetic and functional properties in operating LSCs in an easy and straightforward manner. In particular, the self-healing response of these systems may become crucial in the presence of multiple surface scratches, which would be expected to yield a significant device performance drop. To investigate this aspect, a set of LSCs with increasing number of surface damages were prepared and their performance after both scratching and light-induced healing cycles were recorded as a function of the damage level. These experiments were carried out only on LR305/PU-Cou LSC devices, as it was previously demonstrated that the addition of the luminophore into the PU-Cou matrix does not affect the photo-induced healing response of the coating. As illustrated in **Figure 8A**, the presence of a higher number of surface cuts led to a sharper drop in  $\eta_{LSC}$  compared with the single-scratch system (namely a  $\sim 5\%$  and  $\sim 11\%$  loss in  $\eta_{LSC}$  for single-

scratch and multiple-scratch LSC samples, respectively), ascribable to a progressively lower ability to trap travelling photons within the waveguide. Interestingly, after irradiation treatment the multiple surface scratches were completely repaired and the  $\eta_{LSC}$  of the correspondingly healed LSC devices resulted to be comparable to that obtained on pristine samples. This effect could be attributed to the ability of the [2+2] photoreversible cycloaddition reaction occurring at molecular level to reestablish the original surface smoothness of the coating, as demonstrated by the results of profilometric analysis (Figure S7 and Figure S8 in Supporting Information).

Finally, the performance of large-area LSC samples damaged with multiple scratches and healed *via* the proposed light-exposure treatment was evaluated to elucidate the role of mechanically-induced surface scattering on the overall device efficiency for increasing LSC dimensions. More specifically, 5 x 5 cm<sup>2</sup>, 10 x 10 cm<sup>2</sup> and 15 x 15 cm<sup>2</sup> LR305/PU-Cou LSCs were produced and the value of  $\eta_{LSC}$  in pristine, damaged and healed LSC devices with different dimensions was recorded. To ensure reproducibility, the same scratch pattern was used on all LSCs to obtain the same level of surface damage, as schematically depicted in **Figure 8B**. Interestingly, a clear reduction in  $\eta_{LSC}$  values was observed for scratched LSCs of increasing dimension. This confirms the detrimental effect of the presence of imperfections and optical defects at the waveguide/air interface on LSC performance even in the case of larger-area LSC devices, thus further highlighting the relevance of the photo-responsive polymer matrix presented in this work also in real larger-scale applications

#### 4. Conclusion

In conclusion, a coumarin based, photo-responsive polymer coating exhibiting excellent UV-induced self-healing capabilities was demonstrated in this work for application as host matrix in thin-film LSC devices. This crosslinked polymeric system is characterized by high optical transmittance (> 90%) in the visible spectrum and by remarkable molecular reversibility, which results in outstanding light-induced self-healing behavior. Indeed, healing of surface scratches could be possible by sole UV irradiation, with no need for additional thermal treatment.

LSC devices based on such photo-responsive coatings incorporating suitable luminescent species yielded PV performance comparable with reference thin-film LSCs based on state-of-the-art matrices (i.e., PMMA), thus ranking this functional LSC platform among the best performing systems in the field, with the valuable advantage of providing additional light-induced healing ability. In particular, the decline in PV performance experienced by mechanically scratched LSCs could be fully recovered upon a suitable UV irradiation cycle, as a result of the successful healing process provided by the reversible [2+2] cleavage/dimerization photo-cycloaddition of the coumarin-based moiety.

This work provides the first demonstration of optically transparent, photo-reversible polymeric host matrices for LSCs with high efficiency and excellent healing capabilities, thus enabling the development of stimuli-responsive durable LSC devices with added functionality.

## ASSOCIATED CONTENT

### Supporting Information

Supporting Information is available from the free of charge at

PU-Cou synthesis monitored by FTIR, DSC of pristine and crosslinked PU-Cou, TGA of crosslinked PU-Cou, Weathering test of undoped crosslinked PU-Cou, Photo-induced reversibility of the polymer network monitored by FTIR, Self-healing, Extraction in solvent, Fluorescence resonance energy transfer (FRET), C6/PU-Cou as-cast/crosslinked coatings at different luminophore concentrations and Effect of repeated UV irradiation.

## AUTHOR INFORMATION

### Corresponding Author

\*E-mail: [gianmarco.griffini@polimi.it](mailto:gianmarco.griffini@polimi.it)

### ORCID iDs

Giovanni Fortunato: 0000-0002-8922-8081  
Francesca Corsini: 0000-0002-9109-3737  
Stefano Turri: 0000-0001-8996-0603  
Gianmarco Griffini: 0000-0002-9924-1722

## Notes

The authors declare no competing financial interest.

## ACKNOWLEDGMENTS

Authors greatly acknowledge Gigliola Clerici for her kind support with DSC analysis.

## REFERENCES

- (1) Biyik, E.; Araz, M.; Hepbasli, A.; Shahrestani, M.; Yao, R.; Shao, L.; Essah, E.; Oliveira, A. C.; del Caño, T.; Rico, E.; Lechón, J. L.; Andrade, L.; Mendes, A.; Atlı, Y. B. A Key Review of Building Integrated Photovoltaic (BIPV) Systems. *Eng. Sci. Technol. an Int. J.* **2017**, *20*, 833–858. <https://doi.org/10.1016/j.jestch.2017.01.009>.
- (2) Debije, M. G.; Verbunt, P. P. C. Thirty Years of Luminescent Solar Concentrator Research: Solar Energy for the Built Environment. *Adv. Energy Mater.* **2012**, *2*, 12–35. <https://doi.org/10.1002/aenm.201100554>.
- (3) Meinardi, F.; Bruni, F.; Brovelli, S. Luminescent Solar Concentrators for Building-Integrated Photovoltaics. *Nat. Rev. Mater.* **2017**, *2*, 1–9. <https://doi.org/10.1038/natrevmats.2017.72>.
- (4) Traverse, C. J.; Pandey, R.; Barr, M. C.; Lunt, R. R. Emergence of Highly Transparent Photovoltaics for Distributed Applications. *Nat. Energy* **2017**, *2*, 849–860. <https://doi.org/10.1038/s41560-017-0016-9>.
- (5) Griffini, G. Host Matrix Materials for Luminescent Solar Concentrators: Recent Achievements and Forthcoming Challenges. *Front. Mater.* **2019**, *6*, 1–8. <https://doi.org/10.3389/fmats.2019.00029>.
- (6) McKenna, B.; Evans, R. C. Towards Efficient Spectral Converters through Materials Design for Luminescent Solar Devices. *Adv. Mater.* **2017**, *29*, 1606491. <https://doi.org/10.1002/adma.201606491>.
- (7) Pucci, A. Luminescent Solar Concentrators Based on Aggregation Induced Emission. *Isr. J. Chem.* **2018**, *58*, 837–844. <https://doi.org/10.1002/ijch.201800028>.
- (8) Moraitis, P.; Schropp, R. E. I.; Van Sark, W. G. J. H. . Nanoparticles for Luminescent Solar Concentrators - A Review. *Opt. Mater.* **2018**, *84*, 636–645. <https://doi.org/10.1016/j.optmat.2018.07.034>.
- (9) Zhou, Y.; Zhao, H.; Ma, D.; Rosei, F. Harnessing the Properties of Colloidal Quantum Dots in Luminescent Solar Concentrators. *Chem. Soc. Rev.* **2018**, *47*, 5866–5890. <https://doi.org/10.1039/c7cs00701a>.
- (10) Griffini, G.; Brambilla, L.; Levi, M.; Castiglioni, C.; Del Zoppo, M.; Turri, S. Anthracene/Tetracene Cocrystals as Novel Fluorophores in Thin-Film Luminescent Solar Concentrators. *RSC Adv.* **2014**, *4*, 9893–9897. <https://doi.org/10.1039/c3ra46810k>.
- (11) Zettl, M.; Mayer, O.; Klampaftis, E.; Richards, B. S. Investigation of Host Polymers for Luminescent Solar Concentrators. *Energy Technol.* **2017**, *5*, 1037–1044. <https://doi.org/10.1002/ente.201600498>.
- (12) Tummeltshammer, C.; Taylor, A.; Kenyon, A. J.; Papakonstantinou, I. Losses in Luminescent

- Solar Concentrators Unveiled. *Sol. Energy Mater. Sol. Cells* **2016**, *144*, 40–47. <https://doi.org/10.1016/j.solmat.2015.08.008>.
- (13) Thomas, W. R. L.; Drake, J. M.; Lesiecki, M. L. Light Transport in Planar Luminescent Solar Concentrators: The Role of Matrix Losses. *Appl. Opt.* **1983**, *22*, 3440. <https://doi.org/10.1364/ao.22.003440>.
  - (14) Zhang, F.; Ju, P.; Pan, M.; Zhang, D.; Huang, Y.; Li, G.; Li, X. Self-Healing Mechanisms in Smart Protective Coatings: A Review. *Corros. Sci.* **2018**, *144*, 74–88. <https://doi.org/10.1016/j.corsci.2018.08.005>.
  - (15) Delgado-Sanchez, J. M. Luminescent Solar Concentrators: Photo-Stability Analysis and Long-Term Perspectives. *Sol. Energy Mater. Sol. Cells* **2019**, *202*, 110134. <https://doi.org/10.1016/j.solmat.2019.110134>.
  - (16) Liu, G.; Mazzaro, R.; Wang, Y.; Zhao, H.; Vomiero, A. High Efficiency Sandwich Structure Luminescent Solar Concentrators Based on Colloidal Quantum Dots. *Nano Energy* **2019**, *60*, 119–126. <https://doi.org/10.1016/j.nanoen.2019.03.038>.
  - (17) Zhao, H.; Liu, G.; Han, G. High-Performance Laminated Luminescent Solar Concentrators Based on Colloidal Carbon Quantum Dots. *Nanoscale Adv.* **2019**, *1*, 4888–4894. <https://doi.org/10.1039/c9na00527g>.
  - (18) Liu, X.; Luo, B.; Liu, J.; Jing, D.; Benetti, D.; Rosei, F. Eco-Friendly Quantum Dots for Liquid Luminescent Solar Concentrators. *J. Mater. Chem. A* **2020**, *8*, 1787–1798. <https://doi.org/10.1039/c9ta09586a>.
  - (19) Bergren, M. R.; Makarov, N. S.; Ramasamy, K.; Jackson, A.; Guglielmetti, R.; McDaniel, H. High-Performance CuInS<sub>2</sub> Quantum Dot Laminated Glass Luminescent Solar Concentrators for Windows. *ACS Energy Lett.* **2018**, *3*, 520–525. <https://doi.org/10.1021/acsenergylett.7b01346>.
  - (20) Credi, C.; Pintossi, D.; Bianchi, C. L.; Levi, M.; Griffini, G.; Turri, S. Combining Stereolithography and Replica Molding: On the Way to Superhydrophobic Polymeric Devices for Photovoltaics. *Mater. Des.* **2017**, *133*, 143–153. <https://doi.org/10.1016/j.matdes.2017.07.068>.
  - (21) Pintossi, D.; Colombo, A.; Levi, M.; Dragonetti, C.; Turri, S.; Griffini, G. UV-Curable Fluoropolymers Crosslinked with Functional Fluorescent Dyes: The Way to Multifunctional Thin-Film Luminescent Solar Concentrators. *J. Mater. Chem. A* **2017**, *5*, 9067–9075. <https://doi.org/10.1039/c7ta01692a>.
  - (22) Tatsi, E.; Fortunato, G.; Rigatelli, B.; Lyu, G.; Turri, S.; Evans, R. C.; Griffini, G. Thermoresponsive Host Polymer Matrix for Self-Healing Luminescent Solar Concentrators. *ACS Appl. Energy Mater.* **2020**, *3*, 1152–1160. <https://doi.org/10.1021/acsaem.9b02196>.
  - (23) Vauthier, M.; Jierry, L.; Oliveira, J. C.; Hassouna, L.; Roucoules, V.; Bally-Le Gall, F. Interfacial Thermoreversible Chemistry on Functional Coatings: A Focus on the Diels–Alder Reaction. *Adv. Funct. Mater.* **2019**, *29*, 1–16. <https://doi.org/10.1002/adfm.201806765>.
  - (24) Binder, W. H. *Self-Healing Polymers: From Principles to Applications*; Wiley & Sons, 2013.
  - (25) Yang, Y.; Urban, M. W. Self-Healing Polymeric Materials. *Chem. Soc. Rev.* **2013**, *42*, 7446–7467. <https://doi.org/10.1039/c3cs60109a>.
  - (26) Bekas, D. G.; Tsirka, K.; Baltzis, D.; Paipetis, A. S. Self-Healing Materials: A Review of Advances in Materials, Evaluation, Characterization and Monitoring Techniques. *Compos. Part B Eng.* **2016**, *87*, 92–119. <https://doi.org/10.1016/j.compositesb.2015.09.057>.
  - (27) van der Zwaag, S. An Introduction to Material Design Principles: Damage Prevention versus Damage Management. In *Self Healing Materials: An Alternative Approach to 20 Centuries of Materials Science*; van der Zwaag, S., Ed.; Springer-Verlag Berlin: Berlin, 2007; pp 1–18.
  - (28) Habault, D.; Zhang, H.; Zhao, Y. Light-Triggered Self-Healing and Shape-Memory Polymers. *Chem. Soc. Rev.* **2013**, *42*, 7244–7256. <https://doi.org/10.1039/c3cs35489j>.
  - (29) Kaur, G.; Johnston, P.; Saito, K. Photo-Reversible Dimerisation Reactions and Their Applications in Polymeric Systems. *Polym. Chem.* **2014**, *5*, 2171–2186. <https://doi.org/10.1039/c3py01234d>.

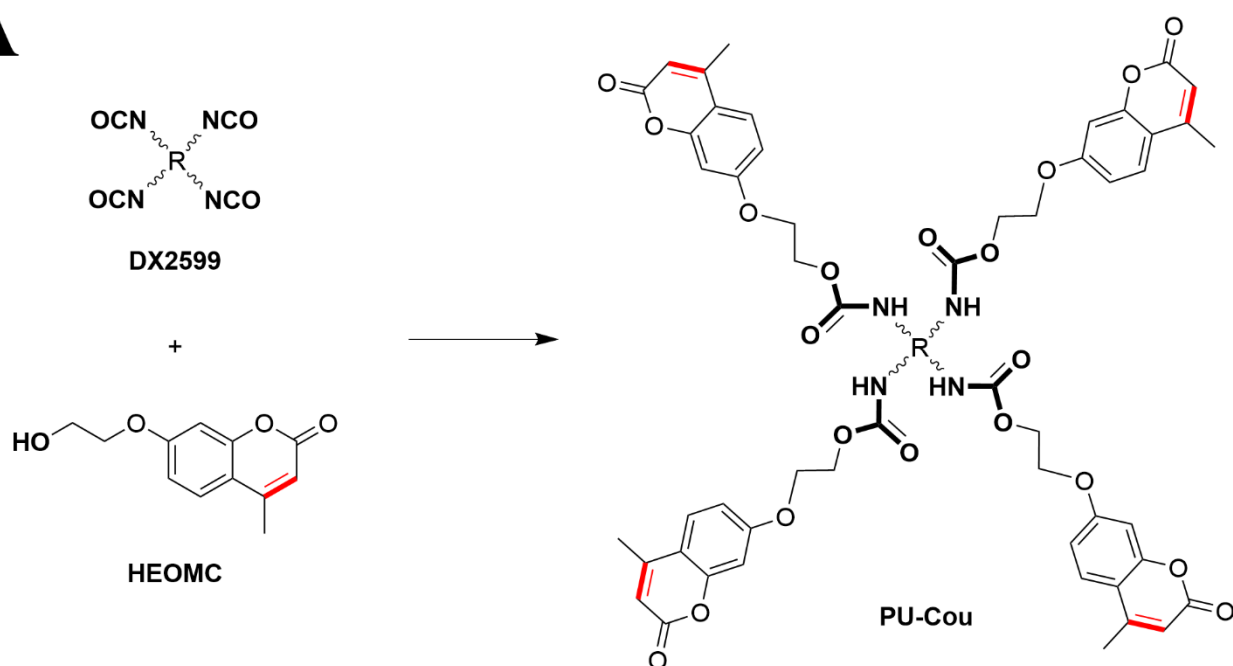
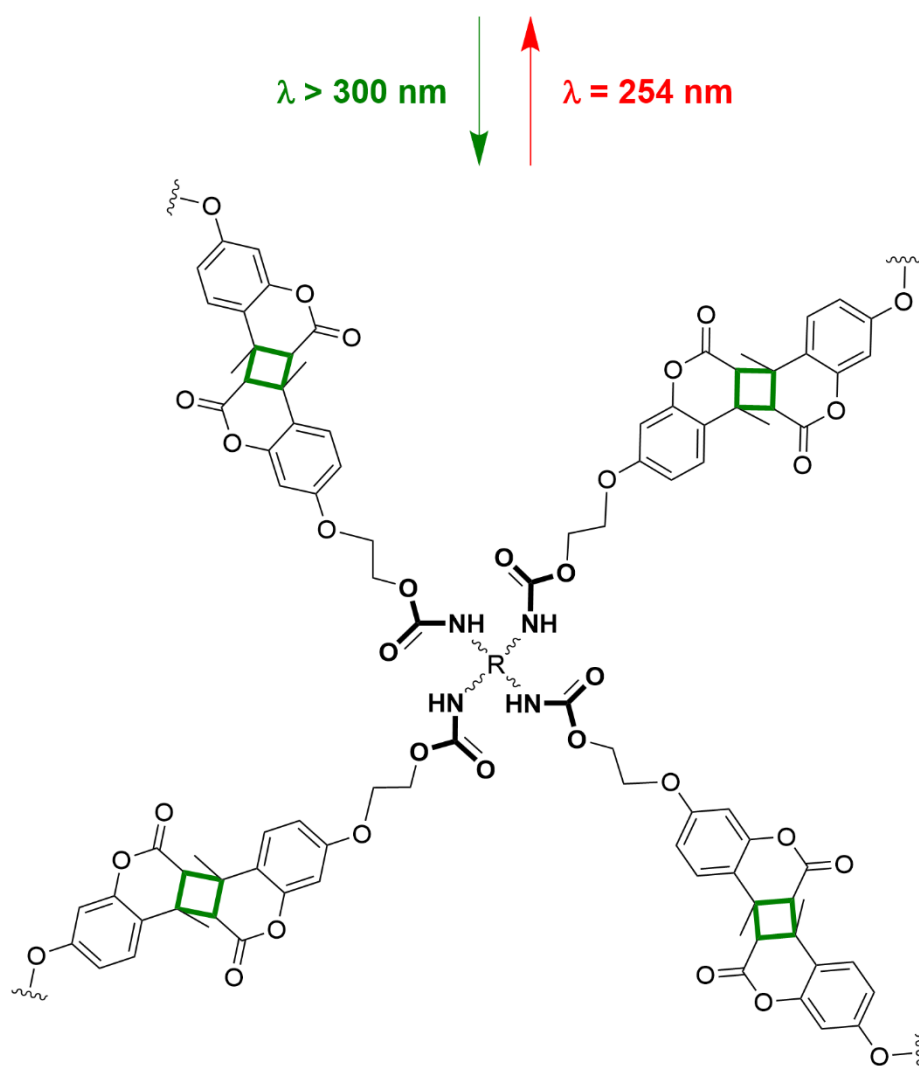
- (30) Frisch, H.; Marschner, D. E.; Goldmann, A. S.; Barner-Kowollik, C. Wavelength-Gated Dynamic Covalent Chemistry. *Angew. Chemie - Int. Ed.* **2018**, *57*, 2036–2045. <https://doi.org/10.1002/anie.201709991>.
- (31) Trenor, S. R.; Shultz, A. R.; Love, B. J.; Long, T. E. Coumarins in Polymers: From Light Harvesting to Photo-Cross-Linkable Tissue Scaffolds. *Chem. Soc. Rev.* **2004**, *104*, 3059–3077.
- (32) Lin, H.; Wan, X.; Jiang, X.; Wang, Q.; Yin, J. A “Thiol-Ene” Photo-Curable Hybrid Fluorinated Resist for the High-Performance Replica Mold of Nanoimprint Lithography (NIL). *J. Mater. Chem.* **2012**, *22*, 2616–2623. <https://doi.org/10.1039/c1jm13765d>.
- (33) Lu, D.; Zhu, M.; Wu, S.; Wang, W.; Lian, Q.; Saunders, B. R. Triply Responsive Coumarin-Based Microgels with Remarkably Large Photo-Switchable Swelling. *Polym. Chem.* **2019**, *10*, 2516–2526. <https://doi.org/10.1039/c9py00233b>.
- (34) Marturano, V.; Marcille, H.; Cerruti, P.; Bandeira, N. A. G.; Giamberini, M.; Trojanowska, A.; Tylkowski, B.; Carfagna, C.; Ausanio, G.; Ambrogio, V. Visible-Light Responsive Nanocapsules for Wavelength-Selective Release of Natural Active Agents. *ACS Appl. Nano Mater.* **2019**, *2*, 4499–4506. <https://doi.org/10.1021/acsanm.9b00882>.
- (35) Samanta, P.; Kapat, K.; Maiti, S.; Biswas, G.; Dhara, S.; Dhara, D. PH-Labile and Photochemically Cross-Linkable Polymer Vesicles from Coumarin Based Random Copolymer for Cancer Therapy. *J. Colloid Interface Sci.* **2019**, *555*, 132–144. <https://doi.org/10.1016/j.jcis.2019.07.069>.
- (36) Ling, J.; Rong, M. Z.; Zhang, M. Q. Coumarin Imparts Repeated Photochemical Remendability to Polyurethane. *J. Mater. Chem.* **2011**, *21*, 18373–18380. <https://doi.org/10.1039/c1jm13467a>.
- (37) Ling, J.; Rong, M. Z.; Zhang, M. Q. Photo-Stimulated Self-Healing Polyurethane Containing Dihydroxyl Coumarin Derivatives. *Polymer (Guildf).* **2012**, *53*, 2691–2698. <https://doi.org/10.1016/j.polymer.2012.04.016>.
- (38) Aguirresarobe, R. H.; Martin, L.; Aramburu, N.; Irusta, L.; Fernandez-Berridi, M. J. Coumarin Based Light Responsive Healable Waterborne Polyurethanes. *Prog. Org. Coatings* **2016**, *99*, 314–321. <https://doi.org/10.1016/j.porgcoat.2016.06.011>.
- (39) Seoane Rivero, R.; Bilbao Solaguren, P.; Gondra Zubieta, K.; Peponi, L.; Marcos-Fernández, A. Synthesis, Kinetics of Photo-Dimerization/Photo-Cleavage and Physical Properties of Coumarin-Containing Branched Polyurethanes Based on Polycaprolactones. *Express Polym. Lett.* **2016**, *10*, 84–95. <https://doi.org/10.3144/expresspolymlett.2016.10>.
- (40) Abdallh, M.; Hearn, M. T. W.; Simon, G. P.; Saito, K. Light Triggered Self-Healing of Polyacrylate Polymers Crosslinked with 7-Methacryloyoxycoumarin Crosslinker. *Polym. Chem.* **2017**, *8*, 5875–5883. <https://doi.org/10.1039/c7py01385j>.
- (41) Wang, J. P.; Wang, J. K.; Zhou, Q.; Li, Z.; Han, Y.; Song, Y.; Yang, S.; Song, X.; Qi, T.; Möhwald, H.; Shchukin, D.; Li, G. L. Adaptive Polymeric Coatings with Self-Reporting and Self-Healing Dual Functions from Porous Core–Shell Nanostructures. *Macromol. Mater. Eng.* **2018**, *303*, 1–9. <https://doi.org/10.1002/mame.201700616>.
- (42) Abdallh, M.; Yoshikawa, C.; Hearn, M. T. W.; Simon, G. P.; Saito, K. Photoreversible Smart Polymers Based on  $2\pi + 2\pi$  Cycloaddition Reactions: Nanofilms to Self-Healing Films. *Macromolecules* **2019**, *52*, 2446–2455. <https://doi.org/10.1021/acs.macromol.8b01729>.
- (43) Hughes, T.; Simon, G. P.; Saito, K. Photocuring of 4-Arm Coumarin-Functionalised Monomers to Form Highly Photoreversible Crosslinked Epoxy Coatings. *Polym. Chem.* **2019**, *10*, 2134–2142. <https://doi.org/10.1039/c8py01767k>.
- (44) Wang, Y.; Liu, Q.; Li, J.; Ling, L.; Zhang, G.; Sun, R.; Wong, C. P. UV-Triggered Self-Healing Polyurethane with Enhanced Stretchability and Elasticity. *Polymer*. **2019**, *172*, 187–195. <https://doi.org/10.1016/j.polymer.2019.03.045>.
- (45) Wong, C. S.; Hassan, N. I.; Su’ait, M. S.; Pelach Serra, M. A.; Mendez Gonzalez, J. A.; Granda, L. A.; Badri, K. H. Photo-Activated Self-Healing Bio-Based Polyurethanes. *Ind. Crops Prod.* **2019**, *140*, 111613. <https://doi.org/10.1016/j.indcrop.2019.111613>.
- (46) Kiskan, B.; Yagci, Y. Self-Healing of Poly(Propylene Oxide)-Polybenzoxazine Thermosets by

- Photoinduced Coumarine Dimerization. *J. Polym. Sci. Part A Polym. Chem.* **2014**, *52*, 2911–2918. <https://doi.org/10.1002/pola.27323>.
- (47) Banerjee, S.; Tripathy, R.; Cozzens, D.; Nagy, T.; Keki, S.; Zsuga, M.; Faust, R. Photoinduced Smart, Self-Healing Polymer Sealant for Photovoltaics. *ACS Appl. Mater. Interfaces* **2015**, *7*, 2064–2072. <https://doi.org/10.1021/am508096c>.
- (48) Owens, D. K.; Wendt, R. C. Estimation of the Surface Free Energy of Polymers. *J. Appl. Polym. Sci.* **1969**, *13*, 1741–1747.
- (49) Arnold, R. G.; Nelson, J. A.; Verbanc, J. J. Recent Advances in Isocyanate Chemistry. *Chem. Rev.* **1957**, *57*, 47–76. <https://doi.org/10.1021/cr50013a002>.
- (50) Kuş, N.; Breda, S.; Reva, I.; Tasal, E.; Ogretir, C.; Fausto, R. FTIR Spectroscopic and Theoretical Study of the Photochemistry of Matrix-Isolated Coumarin. *Photochem. Photobiol.* **2007**, *83*, 1237–1253. <https://doi.org/10.1111/j.1751-1097.2007.00152.x>.
- (51) Abu-Eittah, R.; Moustafa, H.; Al-Omar, A. M. The Electronic Absorption Spectra of Some N-Sulfinylanilines. A Molecular Orbital Treatment. *Can. J. Chem.* **1997**, *75*, 934–941. <https://doi.org/10.1139/v97-112>.
- (52) Donovalová, J.; Cigán, M.; Stankovičová, H.; Gašpar, J.; Danko, M.; Gáplovský, A.; Hrdlovič, P. Spectral Properties of Substituted Coumarins in Solution and Polymer Matrices. *Molecules* **2012**, *17*, 3259–3276. <https://doi.org/10.3390/molecules17033259>.
- (53) Ling, J.; Rong, M. Z.; Zhang, M. Q. Effect of Molecular Weight of PEG Soft Segments on Photo-Stimulated Self-Healing Performance of Coumarin Functionalized Polyurethanes. *Chinese J. Polym. Sci.* **2014**, *32*, 1286–1297. <https://doi.org/10.1007/s10118-014-1522-x>.
- (54) Korchia, L.; Bouilhac, C.; Aubert, A.; Robin, J.; Lapinte, V. Light-Switchable Nanoparticles Based on Amphiphilic Diblock, Triblock and Heterograft. *RSC Adv.* **2017**, *7*, 42690–42698. <https://doi.org/10.1039/c7ra07094b>.
- (55) Trovati, G.; Sanches, E. A.; Neto, S. C.; Mascarenhas, Y. P.; Chierice, G. O. Characterization of Polyurethane Resins by FTIR, TGA, and XRD. *J. Appl. Polym. Sci.* **2010**, *115*, 263–268. <https://doi.org/10.1002/app>.
- (56) Rosu, D.; Rosu, L.; Cascaval, C. N. IR-Change and Yellowing of Polyurethane as a Result of UV Irradiation. *Polym. Degrad. Stab.* **2009**, *94*, 591–596. <https://doi.org/10.1016/j.polymdegradstab.2009.01.013>.
- (57) Griffini, G.; Levi, M.; Turri, S. Thin Film Luminescent Solar Concentrators with Improved Light-Exposure Stability. *2014 14th Int. Conf. Environ. Electr. Eng. IEEEIC 2014 - Conf. Proc.* **2014**, 97–101. <https://doi.org/10.1109/IEEEIC.2014.6835844>.
- (58) Carlotti, M.; Ruggeri, G.; Bellina, F.; Pucci, A. Enhancing Optical Efficiency of Thin-Film Luminescent Solar Concentrators by Combining Energy Transfer and Stacked Design. *J. Lumin.* **2016**, *171*, 215–220. <https://doi.org/10.1016/j.jlumin.2015.11.010>.
- (59) Babusca, D.; Benchea, A. C.; Dimitriu, D. G.; Dorohoi, D. O. Spectral and Quantum Mechanical Characterization of 3-(2-Benzothiazolyl)-7-(Diethylamino) Coumarin (Coumarin 6) in Binary Solution. *Anal. Lett.* **2017**, *50*, 2740–2754. <https://doi.org/10.1080/00032719.2017.1300589>.
- (60) Sottile, M.; Tomei, G.; Borsacchi, S.; Martini, F.; Geppi, M.; Ruggeri, G.; Pucci, A. Epoxy Resin Doped with Coumarin 6: Example of Accessible Luminescent Collectors. *Eur. Polym. J.* **2017**, *89*, 23–33. <https://doi.org/10.1016/j.eurpolymj.2017.02.003>.
- (61) Griffini, G.; Brambilla, L.; Levi, M.; Zoppo, M. Del; Turri, S. Photo-Degradation of a Perylene-Based Organic Luminescent Solar Concentrator: Molecular Aspects and Device Implications. *Sol. Energy Mater. Sol. Cells* **2013**, *111*, 41–48. <https://doi.org/10.1016/j.solmat.2012.12.021>.
- (62) Rechthaler, K.; Köhler, G. Excited State Properties and Deactivation Pathways of 7-Aminocoumarins. *Chem. Phys.* **1994**, *189*, 99–116. [https://doi.org/10.1016/0301-0104\(94\)80010-3](https://doi.org/10.1016/0301-0104(94)80010-3).
- (63) Wu, W.; Cao, Z.; Zhao, Y. Theoretical Studies on Absorption, Emission, and Resonance Raman Spectra of Coumarin 343 Isomers. *J. Chem. Phys.* **2012**, *136*.

<https://doi.org/10.1063/1.3693264>.

- (64) Berney, C.; Danuser, G. FRET or No FRET: A Quantitative Comparison. *Biophys. J.* **2003**, *84*, 3992–4010. [https://doi.org/10.1016/S0006-3495\(03\)75126-1](https://doi.org/10.1016/S0006-3495(03)75126-1).
- (65) Clapp, A. R.; Medintz, I. L.; Mauro, J. M.; Fisher, B. R.; Bawendi, M. G.; Mattoussi, H. Fluorescence Resonance Energy Transfer between Quantum Dot Donors and Dye-Labeled Protein Acceptors. *J. Am. Chem. Soc.* **2004**, *126*, 301–310. <https://doi.org/10.1021/ja037088b>.
- (66) Bailey, S. T.; Lokey, G. E.; Hanes, M. S.; Shearer, J. D. M.; McLafferty, J. B.; Beaumont, G. T.; Baseler, T. T.; Layhue, J. M.; Broussard, D. R.; Zhang, Y. Z.; Wittmershaus, B. P. Optimized Excitation Energy Transfer in a Three-Dye Luminescent Solar Concentrator. *Sol. Energy Mater. Sol. Cells* **2007**, *91*, 67–75. <https://doi.org/10.1016/j.solmat.2006.07.011>.
- (67) Lakowicz, J. R. Energy Transfer. In *Principles of Fluorescence Spectroscopy*; Springer Science & Business Media, 2013; pp 368–394.
- (68) Lyu, G.; Kendall, J.; Meazzini, I.; Preis, E.; Bayseç, S.; Scherf, U.; Clément, S.; Evans, R. C. Luminescent Solar Concentrators Based on Energy Transfer from an Aggregation-Induced Emitter Conjugated Polymer. *ACS Appl. Polym. Mater.* **2019**, *1*, 3039–3047. <https://doi.org/10.1021/acsapm.9b00718>.
- (69) Balaban, B.; Doshay, S.; Osborn, M.; Rodriguez, Y.; Carter, S. A. The Role of FRET in Solar Concentrator Efficiency and Color Tunability. *J. Lumin.* **2014**, *146*, 256–262. <https://doi.org/10.1016/j.jlumin.2013.09.049>.
- (70) Al-Kaysi, R. O.; Sang Ahn, T.; Müller, A. M.; Bardeen, C. J. The Photophysical Properties of Chromophores at High (100 M and above) Concentrations in Polymers and as Neat Solids. *Phys. Chem. Chem. Phys.* **2006**, *8*, 3453–3459. <https://doi.org/10.1039/b605925b>.
- (71) Haines, C.; Chen, M.; Ghiggino, K. P. The Effect of Perylene Diimide Aggregation on the Light Collection Efficiency of Luminescent Concentrators. *Sol. Energy Mater. Sol. Cells* **2012**, *105*, 287–292. <https://doi.org/10.1016/j.solmat.2012.06.030>.
- (72) Yoo, H.; Yang, J.; Yousef, A.; Wasielewski, M. R.; Kim, D. Excimer Formation Dynamics of Intramolecular  $\pi$ -Stacked Perylenediimides Probed by Single-Molecule Fluorescence Spectroscopy. *J. Am. Chem. Soc.* **2010**, *132*, 3939–3944. <https://doi.org/10.1021/ja910724x>.
- (73) Banal, J. L.; White, J. M.; Lam, T. W.; Blakers, A. W.; Ghiggino, K. P.; Wong, W. W. H. A Transparent Planar Concentrator Using Aggregates of Gem-Pyrene Ethenes. *Adv. Energy Mater.* **2015**, *5*, 1–7. <https://doi.org/10.1002/aenm.201500818>.
- (74) Banal, J. L.; Soleimaninejad, H.; Jradi, F. M.; Liu, M.; White, J. M.; Blakers, A. W.; Cooper, M. W.; Jones, D. J.; Ghiggino, K. P.; Marder, S. R.; Smith, T. A.; Wong, W. W. H. Energy Migration in Organic Solar Concentrators with a Molecularly Insulated Perylene Diimide. *J. Phys. Chem. C* **2016**, *120*, 12952–12958. <https://doi.org/10.1021/acs.jpcc.6b04479>.



**A****B**

**Scheme 1.** (A) Functionalization of polyisocyanate (DX2599) with coumarin precursor (HEOMC); (B) Reversible crosslinking of PU-Cou *via* photoinduced [2+2] dimerization of coumarin groups.

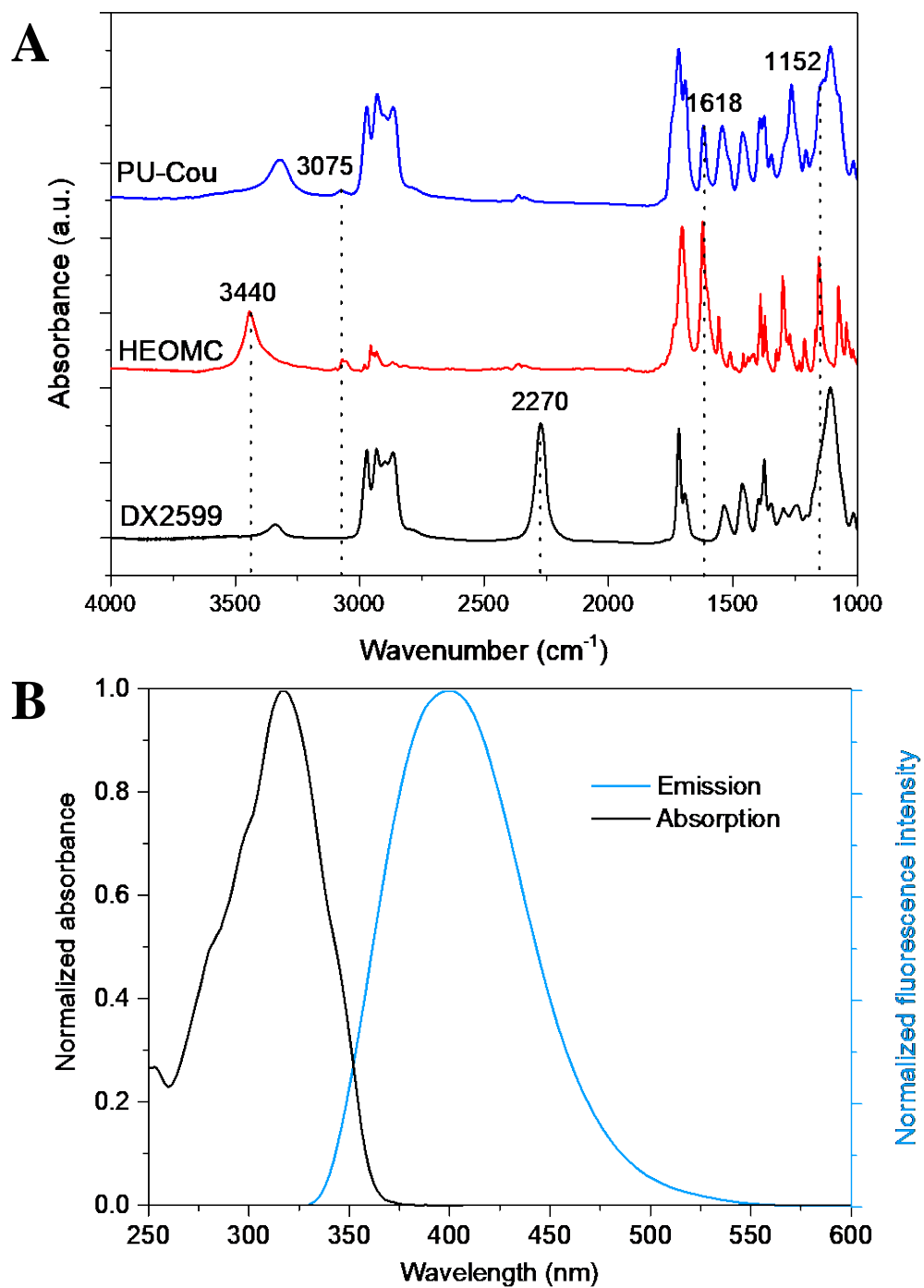


**Figure 1.** (A) FTIR spectra of isocyanate prepolymer (DX2599), 7-(hydroxy ethoxy)-4-methylcoumarin (HEOMC) precursors and coumarin-modified prepolymer (PU-Cou); (B) Normalized UV-Vis absorption and fluorescence emission spectra of PU-Cou.

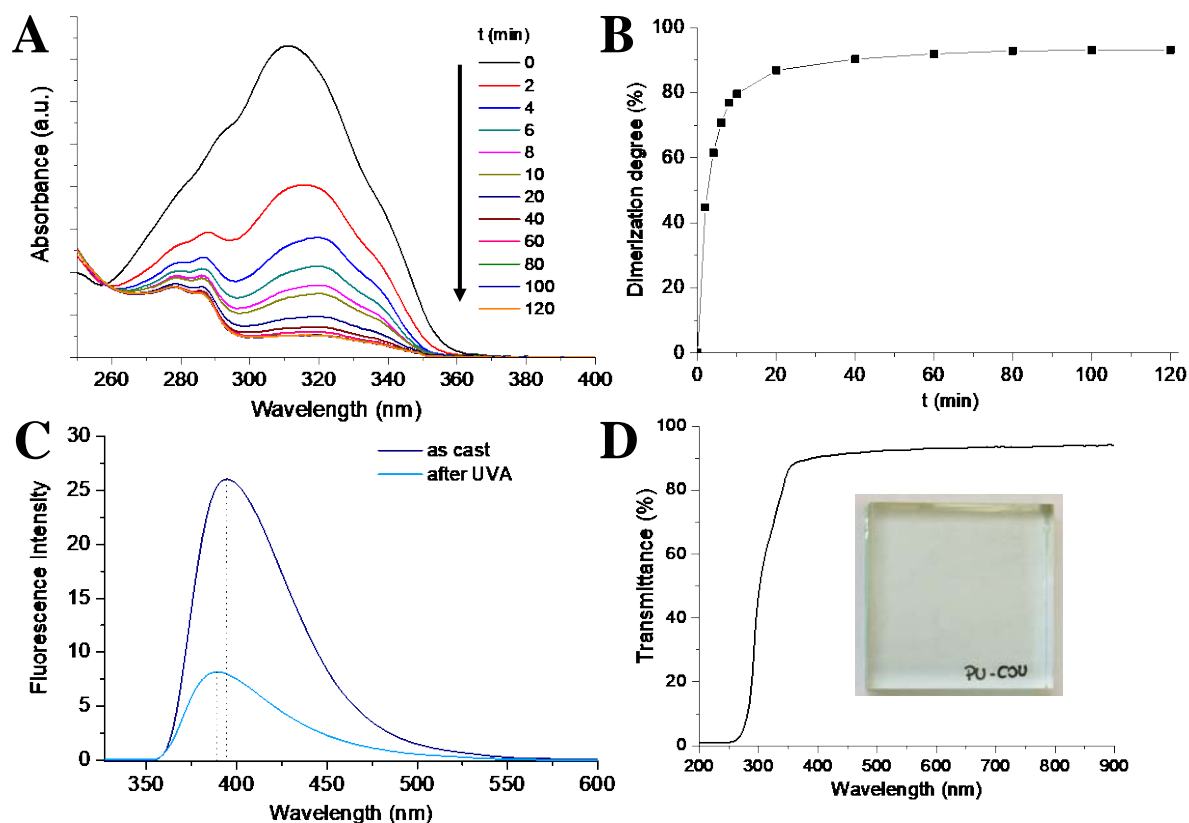


**Figure 2.** (A) UV-Vis absorption spectra of PU-Cou coating and (B) percent conversion of coumarin groups into dimers as a function of different UVA ( $\lambda > 300$  nm) irradiation times; (C) Fluorescence emission spectra of pristine PU-Cou and after UVA irradiation ( $\lambda > 300$  nm, 120 min); (D) UV-Vis transmission spectrum of PU-Cou after irradiation ( $\lambda > 300$  nm, 120 min); in the inset: picture of the crosslinked PU-Cou coated on a glass slab, evidencing its excellent transparency in the visible spectrum.

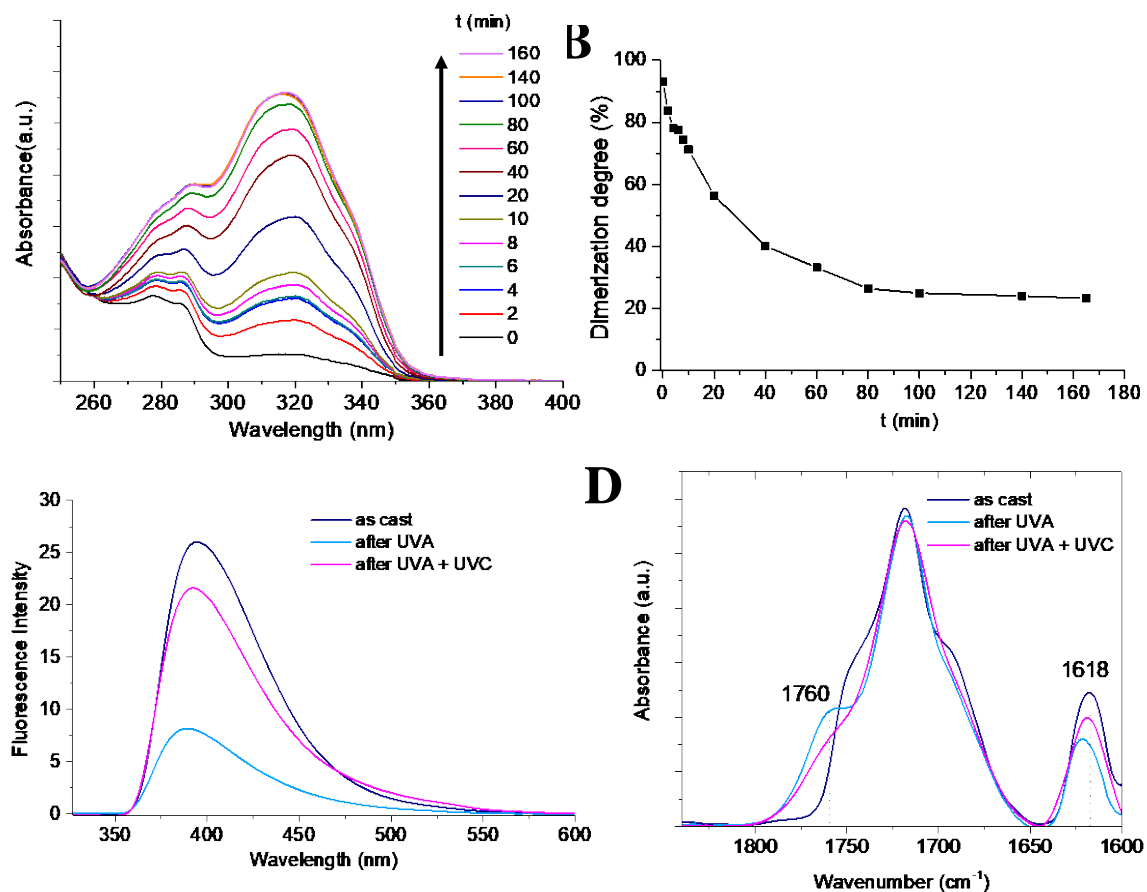


**Figure 3.** (A) UV-Vis absorption spectra of PU-Cou coating and (B) percent conversion of coumarin groups into dimers as a function of different UVC ( $\lambda = 254$  nm) irradiation times; (C) Fluorescence emission spectra and (D) detail of FTIR spectra of pristine PU-Cou, after UVA irradiation ( $\lambda > 300$  nm, 120 min) and after one UVA-UVC ( $\lambda = 254$  nm, 160 min) cycle (signals normalized with respect to the band centered at  $1718 \text{ cm}^{-1}$ ).

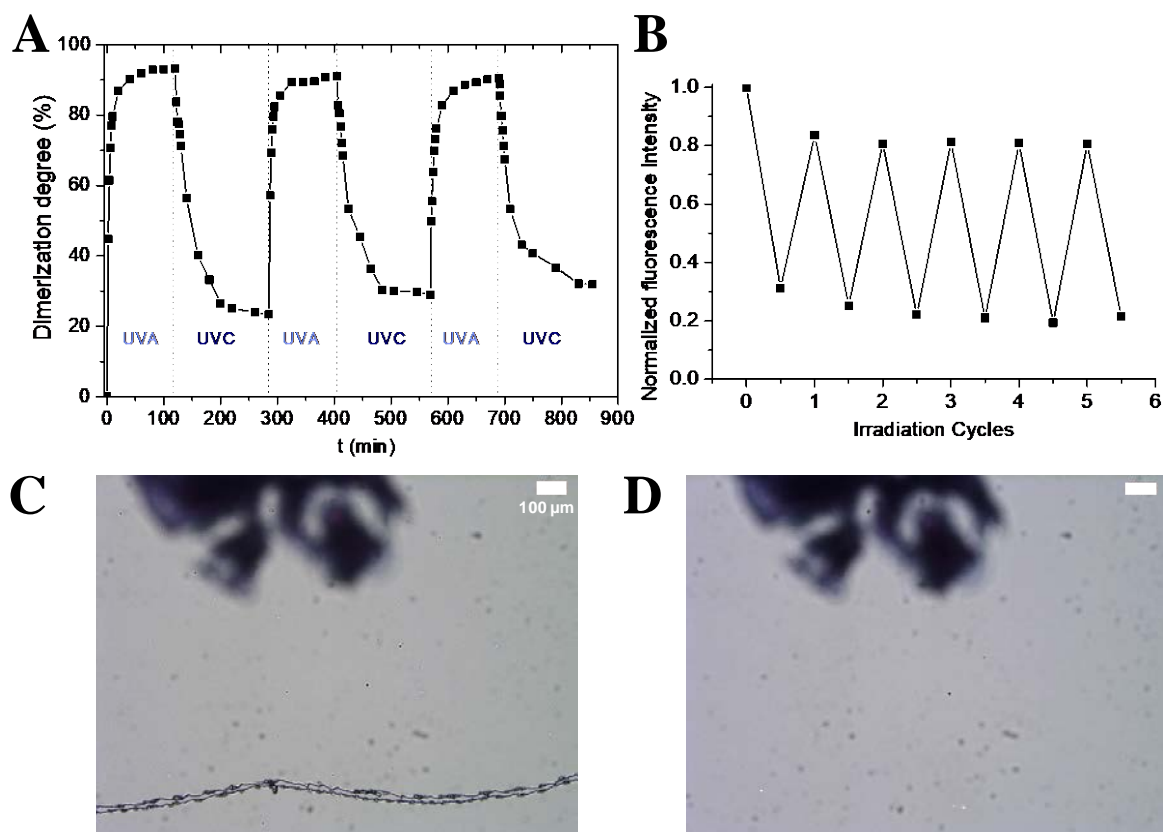


**Figure 4.** (A) Dimerization degree upon alternating exposure under UVA ( $\lambda > 300$  nm, 120 min) and UVC ( $\lambda = 254$  nm, 160 min), calculated from absorption intensity at 320 nm; (B) Fluorescence emission at 394 nm upon subsequent irradiation cycles (UVA+UVC); (C) crosslinked PU-Cou coating damaged with a scalpel; (D) PU-Cou fully repaired after healing treatment (UVC+UVA) at rt.

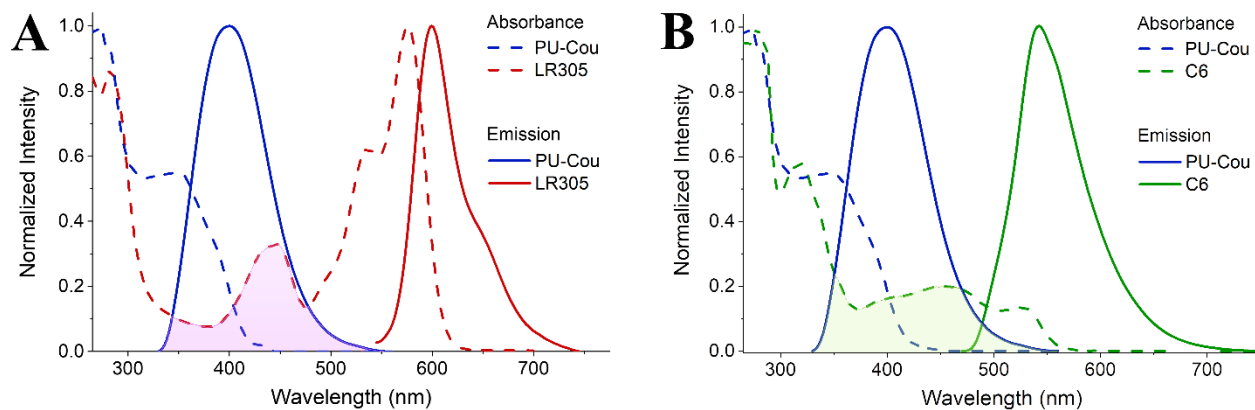


**Figure 5.** Normalized absorption and emission spectra ( $\lambda_{\text{exc}} = 327$  nm) of the undoped crosslinked PU-Cou (donor) compared to the luminophore acceptors (A) LR305 and (B) C6, dispersed in PMMA. The colored areas indicate the overlap between the emission of the donor and the absorption of the acceptor.

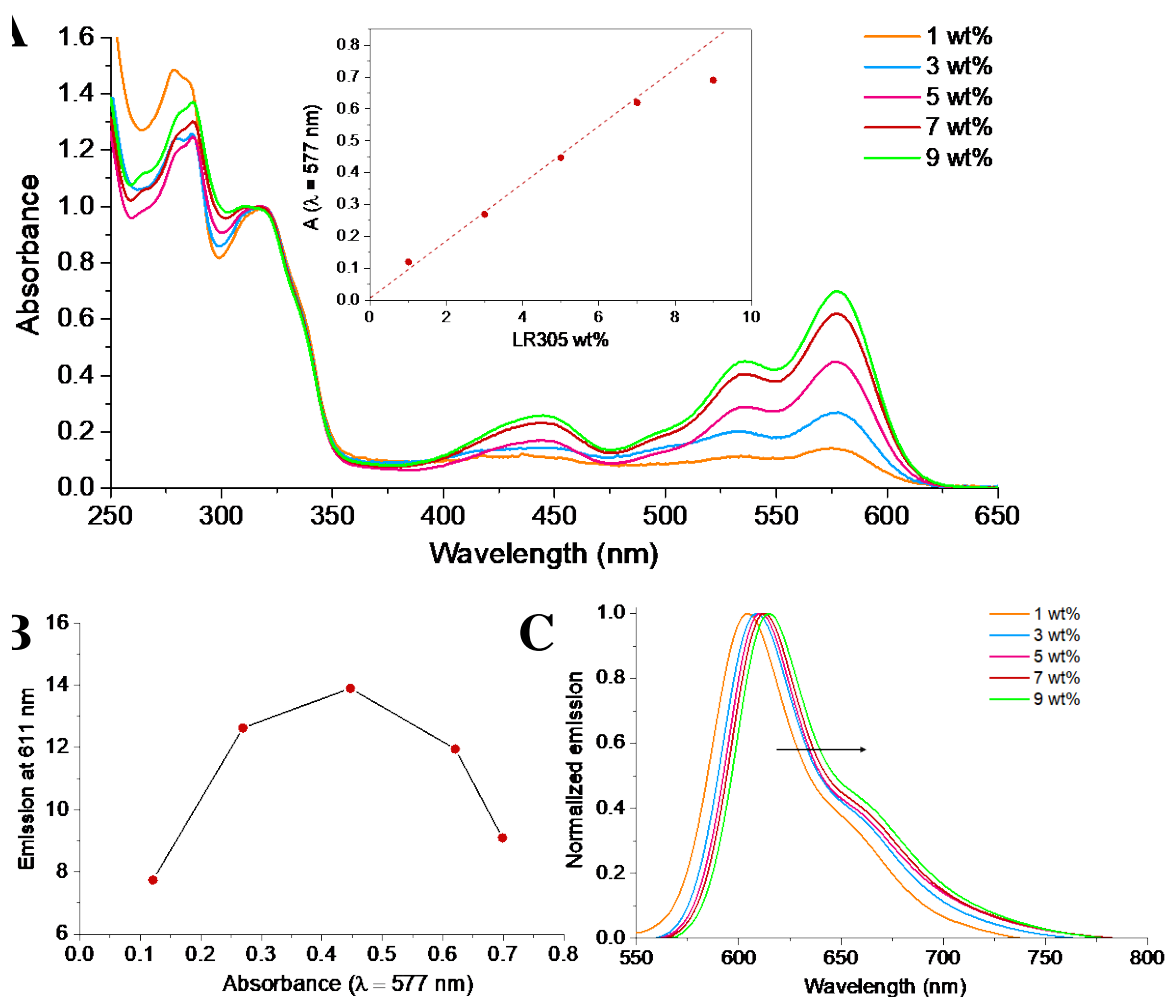


**Figure 6.** Optical properties of crosslinked PU-Cou doped with LR305. (A) UV-Vis absorption spectra at increasing luminophore concentrations; in the inset: absorbance at 577 nm vs. luminophore concentration (dashed line shows linear fit of the experimental data; fitting equation:  $y = 0.09x$ , with  $R^2 = 0.99$ ); (B) Emission intensity at  $\approx 611$  nm peak vs. absorbance at 577 nm. (C) Normalized fluorescence emission spectra at increasing luminophore concentration ( $\lambda_{exc} = 327$  nm).

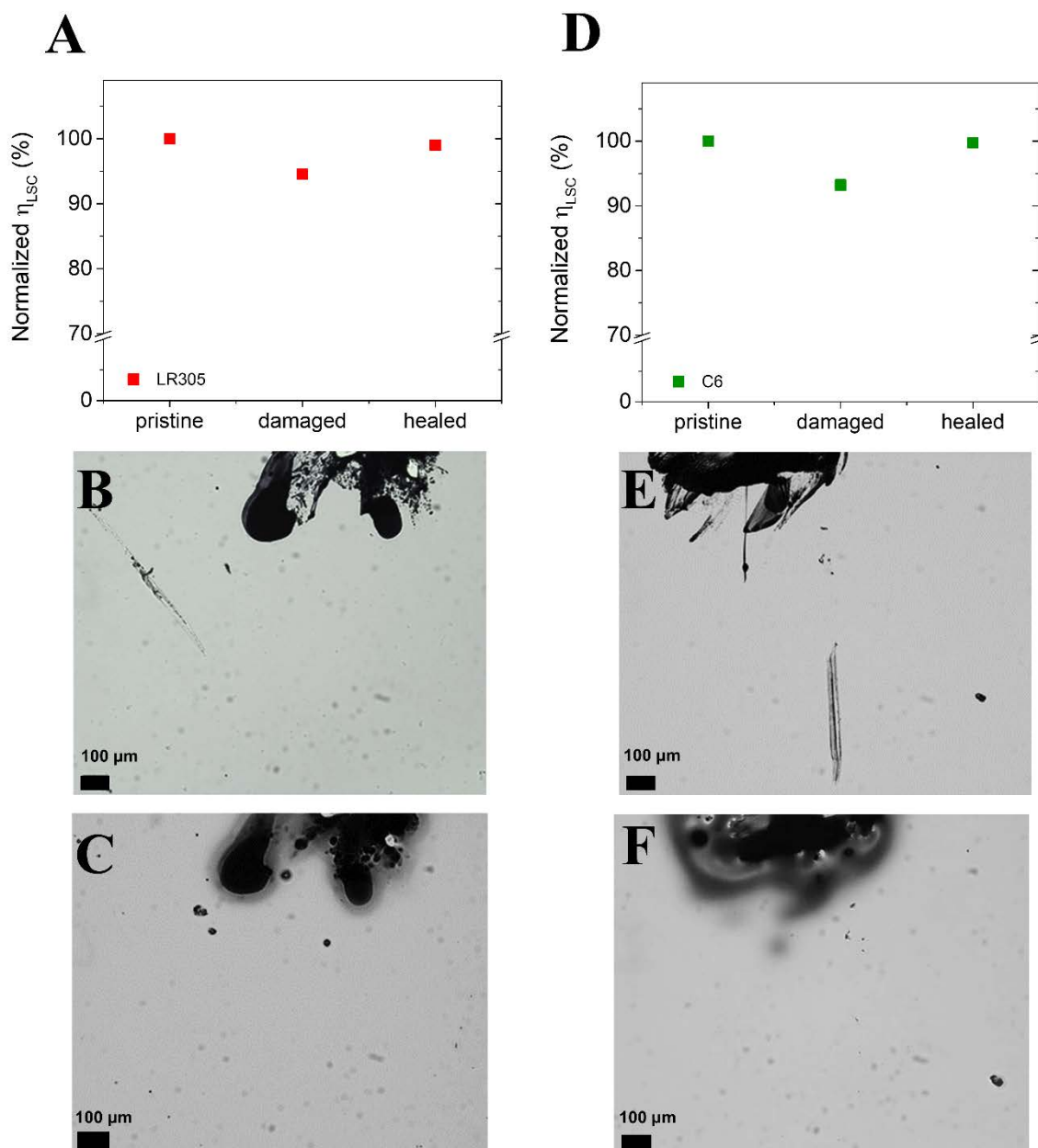


**Figure 7.** (A) and (D) Normalized device efficiency values of photo-reversible PU-Cou matrix doped with 5 wt.% LR305 or 3 wt.% C6, respectively, before the damage, damaged and after UV-induced healing. An appreciable reduction of device performance was detected after damaging the surface of the LSC with a single scratch. The excellent healing capabilities of these systems are to become crucial when a more significant device performance drop is expected as a result of multiple surface scratches. Optical microscope images of LR305/PU-Cou (B) damaged and (C) UV-repaired, and of C6/PU-Cou (E) damaged and (F) UV-repaired.



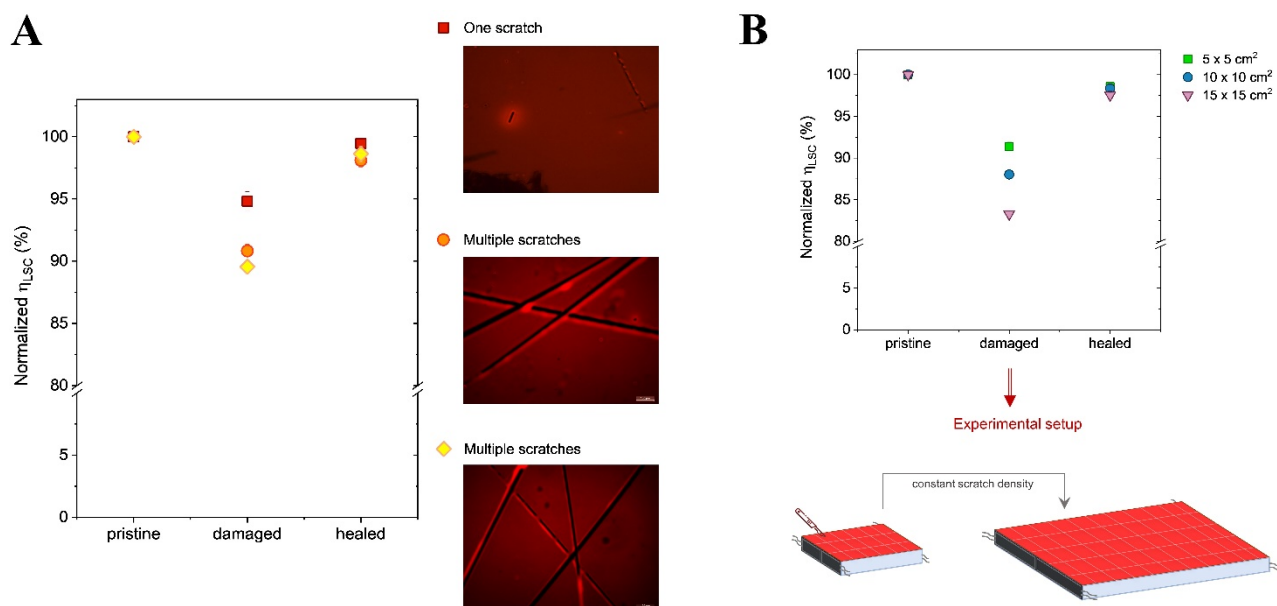


**Figure 8.** (A) Normalized device efficiency values of PU-Cou matrix doped with 5 wt.% LR305 before the damage (pristine), damaged and after UV-induced healing (healed) as a function of the damage level. An increasing reduction of device performance was recorded after damaging the surface of the LSC with a larger number of scratches. Fluorescence microscopy images of corresponding damaged LR305/PU-Cou systems are also reported. (B) Normalized device efficiency values of PU-Cou matrix doped with 5 wt.% LR305 before the damage (pristine), damaged and after UV-induced repair (healed) considering increasingly larger area LSCs (5 x 5 cm<sup>2</sup>, 10 x 10 cm<sup>2</sup> and 15 x 15 cm<sup>2</sup>). As depicted schematically at the bottom, the scratching pattern applied onto 5 x 5 cm<sup>2</sup> LSCs was repeated onto larger-area LSC devices in order to maintain fixed the damage density on LSC with increasing area.

## TABLE OF CONTENT

The first demonstration of a photo-mendable thin-film luminescent solar concentrator is given in this work. The photo-responsive host matrix, obtained by simple UV curing, is highly transparent and exhibits excellent UV-triggered self-healing. The healing cycle allows to restore the original remarkable device efficiency of the dye-doped matrix after a surface damage.

**Keywords:** stimuli-responsive polymers, photo-healable polymers, [2+2] cycloaddition, fluorescent coatings, luminescent solar concentrators

G. Fortunato, E. Tatsi, F. Corsini, S. Turri, and G. Griffini\*

### Stimuli-responsive luminescent solar concentrators based on photo-reversible polymeric systems

